2023 IEEE International Conference on Robotics and Automation (ICRA 2023)
May 29 - June 2, 2023. London, UK

Analytical Approach to Inverse Kinematics of Single Section Mobile Continuum Manipulators

1st Audrey Hyacinthe Bouyom Boutchouang
Dept. Electrical and Telecommunications Engineering
University of Yaoundé I
Yaoundé, Cameroon
bouyom_hyacinthe@yahoo.fr

2nd Achille Melingui
Dept. Electrical and Telecommunications Engineering
University of Yaoundé I
Yaoundé, Cameroon
achillemelingui@gmail.com

3rd J.J.B. Mvogo Ahanda
Dept Electrical and Power Engineering
University of Ebolowa
Ebolowa, Cameroon
josephjeanmvogo@yahoo.fr

4th Xinrui Yang
CRIStAL Laboratory
CNRS-UMR
Villeneuve d'Ascq 59655, France
xinrui.yang@univ-lille.fr

5th Othman Lakhal
CRIStAL Laboratory
CNRS-UMR
Villeneuve d'Ascq 59655, France
othman.lakhal@univ-lille1.fr

6th Frederic Biya Motto
Dept. Physic's
University of Yaoundé I
Yaoundé, Cameroon
biyamotto@yahoo.fr

7th Rochdi Merzouki
CRIStAL Laboratory
CNRS-UMR
Villeneuve d'Ascq 59655, France
rochdi.merzouki@polytech-lille.fr

***Abstract*—This paper proposes a novel mathematical solution to solve the inverse kinematics (IK) of single section mobile continuum manipulators (SSMCMs). Thus, to achieve a given pose of the end-effector (EE), the proposed mathematical solution consists in determining the position and orientation parameters of the mobile platform and of a single section of the continuum manipulator. As advantages, the proposed mathematical solution eliminates the EE pose errors when the dynamic parameters are neglected and the continuum manipulator is cylindrical in shape. A simulation and an experiment validate the proposed approach.**

***Index Terms*—Inverse kinematics (IK), single section mobile continuum manipulator (SSMCM), novel mathematical solution**

I. INTRODUCTION

Compared to the rigid manipulator [1], continuum manipulator [2] is adapted to the application in confined and delicate environments thanks to the soft structure of the continuum manipulator. Moreover, the latter mounted on a mobile platform offers more mobility and flexibility and is suitable for complex applications such as nuclear maintenance [3], space exploration [4], [5], search and rescue operations [6], [7]. However, these applications sometimes impose particular configurations that require high-performance and real-time IK algorithms.

IK consists in determining the parameters of the configuration space of a robot according to a given pose of the EE, when the dynamic parameters of the robot are neglected. Its determination is a difficult problem to solve for the multisection mobile continuum manipulator (MCM) because of the deformable structure of the continuum manipulator which makes it hyper redundant, and the number of additional degrees of freedom brought by the mobile platform. Unlike continuum manipulators where this problem has been widely addressed, very few works have been done for MCMs.

To solve the IK of the Octarm, Li and Xiao [8] proposed an analytical approach of finding a feasible configuration close to the previous configuration of the robot while incorporating environmental constraints and specific constraints on the pose of each section, and assuming that the pose of the platform is known. Liu et al. [7] have proposed the decoupling method to solve the IK of a continuum manipulator mounted on a moving legged platform. On the other hand, numerical methods solve the IK of robots regardless of their number of degrees of freedom and without performing decoupling [9]. As drawbacks, numerical methods depend on the initial configuration and are also confronted with the problems of local minima and singularities which may not only increase the computational time but also generate convergence problems and the infinite loops [10]. Moreover, numerical methods lead to a single solution that can be optimal or not. On the contrary, Boutchouang et al. [9] proposed a clustering-based inverse kinematic model (CIKM) that maintains multiple solutions.

This paper proposes an inverse kinematic model (IKM) based on an analytical approach for SSMCM. The proposed approach consists in mathematically determining the pose

This work has been realized with the support of EU funding through Interreg project CIRMAP NWE 1062.

parameters of the mobile platform and the configuration space parameters of the continuous section. Thus, while the bending plane and curvature angles of the section, and the yaw angle of the mobile platform allow to reach the desired EE orientation, the radius of curvature of the section and the position parameters of the mobile platform allow to reach desired EE position.

The remainder of this article is organized as follows. Section II presents the forward kinematic model (FKM) of the SSMCM. Section III describes the proposed mathematical solution. Sections IV and V present the simulation and experimental results obtained on virtual and real MCMs, respectively. Finally, section VI concludes this work.

II. FORWARD KINEMATIC MODELING OF MCM

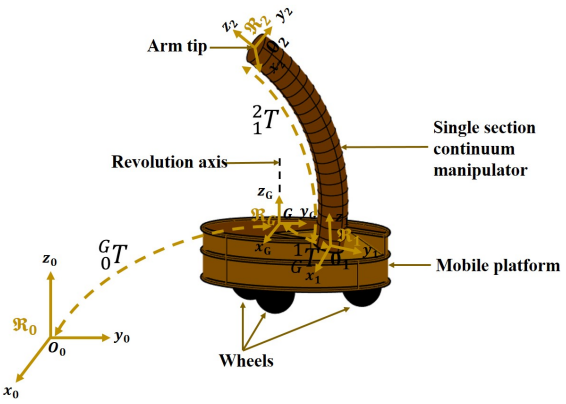

Fig. 1. A single section mobile continuum manipulator. The point G denotes the geometry center of the mobile platform, and the point O_1 its center of mass.

FKM of the SSMCM presented in Fig. 1 can be considered as the composition of the FKM of the mobile platform and the continuum manipulator. In this paper, the platform is assumed omnidirectional. Thus, the FKM of the platform is defined by:

$$ {}^{1}_{0}T(X_G, Y_G, \alpha) = \begin{pmatrix} \cos\alpha & -\sin\alpha & 0 & a\cos\alpha + X_G \\ \sin\alpha & \cos\alpha & 0 & a\sin\alpha + Y_G \\ 0 & 0 & 1 & Z_G \\ 0 & 0 & 0 & 1 \end{pmatrix} \quad (1) $$

where X_G, Y_G, and Z_G are the cartesian coordinates of G relative to the absolute frame $\Re_0$. α denotes the orientation of the mobile platform relative to the absolute frame $\Re_0$ along the z_0-axis, and a is the inter-distance between points G and O_1 in the reference frame $\Re_G$.

FKM of the continuous section is based on the constant curvature approximation (CCA) and is defined by:

$$ {}^{2}_{1}\mathrm{T}(l_{1j}) = {}^{2}_{1}T(\lambda, \theta, \phi) = \begin{pmatrix} c^2\theta c\phi + s^2\theta & c\theta s\theta(c\phi - 1) & c\theta s\phi & \lambda c\theta(1 - c\phi) \\ c\theta s\theta(c\phi - 1) & s^2\theta c\phi + c^2\theta & s\theta s\phi & \lambda s\theta(1 - c\phi) \\ -c\theta s\phi & -s\theta s\phi & c\phi & \lambda s\phi \\ 0 & 0 & 0 & 1 \end{pmatrix} \quad (2) $$

with $c\theta = \cos(\theta)$, $s\theta = \sin(\theta)$, $c\phi = \cos(\phi)$ and $s\phi = \sin(\phi)$.

l_{1j} are the actuator lengths, with $j = 1, 2, 3$ the number of actuators. θ, ϕ and λ denote the angle of the bending plane with respect to the x_1-axis, the angle subtended by the bending arc and the radius of curvature, respectively.

From equations (1) and (2), the FKM of the SSMCM is given by the following expression:

$$ {}^{2}_{0}T(x_G, y_G, \alpha, l_{ij}) = {}^{1}_{0}T(x_G, y_G, \alpha) \times T_t \times {}^{2}_{1}\mathrm{T}(l_{ij}) \quad (3) $$

where T_t is the Homogeneous Transformation Matrix (HTM) defining the tilt of the continuum manipulator on the mobile platform.

From (3), the EE position (X,Y,Z) as well as its orientation (e_0, e_1, e_2, e_3) are determined as follows:

$$ {}^{N+1}_{0}T = \begin{pmatrix} e_{11} & e_{12} & e_{13} & X \\ e_{21} & e_{22} & e_{23} & Y \\ e_{31} & e_{32} & e_{33} & Z \\ 0 & 0 & 0 & 1 \end{pmatrix}, \begin{cases} e_0^2 = \frac{e_{11}+e_{22}+e_{33}+1}{4} \\ e_1 = \frac{e_{32}-e_{23}}{4e_0} \\ e_2 = \frac{e_{13}-e_{31}}{4e_0} \\ e_3 = \frac{e_{21}-e_{12}}{4e_0} \end{cases} \quad (4) $$

with e_{ij} ($i = 1, 2, 3$ and $j = 1, 2, 3$) the components of the rotation matrix of ${}^{N+1}_{0}T$ and e_l ($l = 0, ..., 3$) the euler's parameters.

For more details on the FKM of the SSMCM, interested readers are referred to [9] and [11].

III. PROPOSED INVERSE KINEMATIC MODEL OF MCM

This section starts by the development of the proposed mathematical solution to solve the IK of the SSMCM. The approach consists of first determining the two degrees of rotation of the continuous section and the yaw angle of the mobile platform, respectively. Then, the degree of translation of the continuous section and the position parameters of the mobile platform are successively deduced. It ends with an effectiveness analysis of the proposed mathematical solution.

A. Proposed mathematical solution

Let:

- ${}^{N+1}_{0}T_d$ the HTM constructed from the desired EE pose and defined by :

$$ {}^{N+1}_{0}T_d = \begin{pmatrix} e_{11}^d & e_{12}^d & e_{13}^d & X_d \\ e_{21}^d & e_{22}^d & e_{23}^d & Y_d \\ e_{31}^d & e_{32}^d & e_{33}^d & Z_d \\ 0 & 0 & 0 & 1 \end{pmatrix} \quad (5) $$

  with e_{ij}^d ($i = 1, 2, 3$ and $j = 1, 2, 3$) the components of the rotation matrix and (X_d,Y_d,Z_d) the components of the desired postion.

- ${}^{1}_{0}T_r$ the HTM corresponding to the pose of the mobile platform leading to the desired EE pose. It is defined from the equation (1) as follows:

$$ {}^{1}_{0}T_r = {}^{1}_{0}T(X_{Gr}, Y_{Gr}, \alpha_r) \quad (6) $$

  with α_r, X_{Gr} and Y_{Gr} the pose parameters of the mobile platform to be determined.

- $$T_t = \begin{pmatrix} e_{11}^c & e_{12}^c & e_{13}^c & X_c \\ e_{21}^c & e_{22}^c & e_{23}^c & Y_c \\ e_{31}^c & e_{32}^c & e_{33}^c & Z_c \\ 0 & 0 & 0 & 1 \end{pmatrix} \quad (7)$$

  with e_{ij}^c ($i = 1,2,3$ and $j = 1,2,3$) the components of the rotation matrix and (X_c,Y_c,Z_c) the translation components.
- ${}_1^2T_r$ the HTM corresponding to the configuration of the single section leading to the desired EE pose. It is defined from the equation (2) as follows:

$${}_1^2T_r = {}_1^2T\left(\lambda_r, \theta_r, \phi_r\right) \quad (8)$$

with θ_r, ϕ_r and λ_r the parameters of the continuous section to be determined.

From the FKM of the MCM (4), the relationship between these HTMs is obtained as follows:

$${}_0^2T_d = {}_0^1T_r \times T_t \times {}_1^2T_r \quad (9)$$

By setting $c = \cos$ and $s = \sin$, the development of this relation (9) leads to the following equations:

$$\begin{aligned}&(c^2\theta_r c\phi_r + s^2\theta_r)(e_{11}^c c\alpha_r - e_{21}^c s\alpha_r) + c\theta_r s\theta_r(c\phi_r - 1)\\ &(e_{12}^c c\alpha_r - e_{22}^c s\alpha_r) - c\theta_r s\phi_r(e_{13}^c c\alpha_r - e_{23}^c s\alpha_r) = e_{11}^d\end{aligned} \quad (10)$$

$$\begin{aligned}&(c^2\theta_r c\phi_r + s^2\theta_r)(e_{11}^c s\alpha_r + e_{21}^c c\alpha_r) + c\theta_r s\theta_r(c\phi_r - 1)\\ &(e_{12}^c s\alpha_r + e_{22}^c c\alpha_r) - c\theta_r s\phi_r(e_{13}^c s\alpha_r + e_{23}^c s\alpha_r) = e_{21}^d\end{aligned} \quad (11)$$

$$(c^2\theta_r c\phi_r + s^2\theta_r)e_{31}^c + c\theta_r s\theta_r(c\phi_r - 1)e_{32}^c - e_{33}^c c\theta_r s\phi_r = e_{31}^d \quad (12)$$

$$\begin{aligned}&(s^2\theta_r c\phi_r + c^2\theta_r)(e_{12}^c c\alpha_r - e_{22}^c s\alpha_r) + c\theta_r s\theta_r(c\phi_r - 1)\\ &(e_{11}^c c\alpha_r - e_{21}^c s\alpha_r) - s\theta_r s\phi_r(e_{13}^c c\alpha_r - e_{23}^c s\alpha_r) = e_{12}^d\end{aligned} \quad (13)$$

$$\begin{aligned}&(s^2\theta_r c\phi_r + c^2\theta_r)(e_{12}^c s\alpha_r + e_{22}^c c\alpha_r) + c\theta_r s\theta_r(c\phi_r - 1)\\ &(e_{11}^c s\alpha_r + e_{21}^c c\alpha_r) - s\theta_r s\phi_r(e_{13}^c s\alpha_r + e_{23}^c c\alpha_r) = e_{22}^d\end{aligned} \quad (14)$$

$$(s^2\theta_r c\phi_r + c^2\theta_r)e_{32}^c + c\theta_r s\theta_r(c\phi_r - 1)e_{31}^c - e_{33}^c s\theta_r s\phi_r = e_{32}^d \quad (15)$$

$$\begin{aligned}&c\theta_r s\phi_r(e_{11}^c c\alpha_r - e_{21}^c s\alpha_r) + s\theta_r s\phi_r(e_{12}^c c\alpha_r - e_{22}^c s\alpha_r)\\ &+c\phi_r(e_{13}^c c\alpha_r - e_{23}^c s\alpha_r) = e_{13}^d\end{aligned} \quad (16)$$

$$\begin{aligned}&c\theta_r s\phi_r(e_{11}^c s\alpha_r + e_{21}^c c\alpha_r) + s\theta_r s\phi_r(e_{12}^c s\alpha_r + e_{22}^c c\alpha_r)\\ &+c\phi_r(e_{13}^c s\alpha_r + e_{23}^c c\alpha_r) = e_{23}^d\end{aligned} \quad (17)$$

$$e_{31}^c c\theta_r s\phi_r + e_{32}^c s\theta_r s\phi_r + e_{33}^c c\phi_r = e_{33}^d \quad (18)$$

$$E_1(\theta_r, \phi_r, \alpha_r, \lambda_r) + X_{Gr} = X_d \quad (19)$$

with

$$\begin{aligned}E_1(\theta_r, \phi_r, \alpha_r, \lambda_r) = {}&\lambda_r c\theta_r(e_{11}^c c\alpha_r - e_{21}^c s\alpha_r)(1 - c\phi_r)\\ &+\lambda_r s\theta_r(e_{12}^c c\alpha_r - e_{22}^c s\alpha_r)(1 - c\phi_r)\\ &+\lambda_r s\phi_r(e_{13}^c c\alpha_r - e_{23}^c s\alpha_r) + X_c c\alpha_r - Y_c s\alpha_r + ac\alpha_r\end{aligned}$$

$$E_2(\theta_r, \phi_r, \alpha_r, \lambda_r) + Y_{Gr} = Y_d \quad (20)$$

with

$$\begin{aligned}E_2(\theta_r, \phi_r, \alpha_r, \lambda_r) = {}&\lambda_r c\theta_r(e_{11}^c s\alpha_r + e_{21}^c c\alpha_r)(1 - c\phi_r)\\ &+\lambda_r s\theta_r(e_{12}^c s\alpha_r + e_{22}^c c\alpha_r)(1 - c\phi_r)\\ &+\lambda_r s\phi_r(e_{13}^c c\alpha_r + e_{23}^c s\alpha_r) + X_c s\alpha_r + Y_c c\alpha_r + as\alpha_r\end{aligned}$$

$$\lambda_r E_3(\theta_r, \phi_r) + Z_c + Z_G = Z_d \quad (21)$$

with

$$E_3(\theta_r, \phi_r) = e_{31}^c c\theta_r(1 - c\phi_r) + e_{32}^c s\theta_r(1 - c\phi_r) + e_{33}^c s\phi_r$$

The parameters $\theta_r, \phi_r, \alpha_r, \lambda_r, X_{Gr}$ and Y_{Gr} successively determined as follows:

1) **Calculation of θ_r:** The equations (12) and (15) can be respectively transformed into a system of equations as follows:

$$\begin{cases}\bullet(e_{31}^c c^2\theta_r + e_{32}^c c\theta_r s\theta_r)c\phi_r - e_{33}^c c\theta_r s\phi_r = \\ \qquad e_{31}^d - e_{31}^c s^2\theta_r + e_{32}^c c\theta_r s\theta_r \\ \bullet(e_{32}^c s^2\theta_r + e_{31}^c c\theta_r s\theta_r)c\phi_r - e_{33}^c s\theta_r s\phi_r = \\ \qquad e_{32}^d - e_{32}^c c^2\theta_r + e_{31}^c c\theta_r s\theta_r\end{cases} \quad (22)$$

By multiplying the first and second equations of this system (22) by $s\theta_r$ and $c\theta_r$ respectively, and subtracting them, the following equation is obtained:

$$\begin{aligned}&e_{32}^c c^3\theta_r - e_{31}^c s^3\theta_r - e_{31}^c c^2\theta_r s\theta_r + e_{32}^c c\theta_r s^2\theta_r\\ &-e_{32}^d c\theta_r + e_{31}^d s\theta_r = 0\end{aligned} \quad (23)$$

By replacing $s^2\theta_r = 1 - c^2\theta_r$, in equation (23), the expression of θ_r is given by

$$\theta_r = a\tan 2(e_{32}^c - e_{32}^d, e_{31}^c - e_{31}^d) \quad (24)$$

2) **Calculation of ϕ_r:** By multiplying the first and second equations of this system (22) by e_{31}^c and e_{32}^c respectively, and subtracting them, the following equation is obtained:

$$\begin{aligned}&\left[(e_{31}^c)^2 c^2\theta_r - (e_{32}^c)^2 s^2\theta_r\right] c\phi_r - e_{33}^c(e_{31}^c c\theta_r - e_{32}^c s\theta_r)\\ &s\phi_r = e_{31}^c e_{31}^d - e_{32}^c e_{32}^d + (e_{32}^c)^2 c^2\theta_r - (e_{31}^c)^2 s^2\theta_r\end{aligned} \quad (25)$$

Equations (25) and (18) can be transformed into a system of equations as follows:

$$\begin{cases}\bullet\left[(e_{31}^c)^2 c^2\theta_r - (e_{32}^c)^2 s^2\theta_r\right] c\phi_r - e_{33}^c(e_{31}^c c\theta_r \\ -e_{32}^c s\theta_r)s\phi_r = e_{31}^c e_{31}^d - e_{32}^c e_{32}^d + (e_{32}^c)^2 c^2\theta_r \\ -(e_{31}^c)^2 s^2\theta_r \\ \bullet\ e_{33}^c c\phi_r + (e_{31}^c c\theta_r + e_{32}^c s\theta_r)s\phi_r = e_{33}^d\end{cases} \quad (26)$$

Solving this system (26) leads to the following expressions for $s\phi_r$ and $c\phi_r$:

$$s\phi_r = \frac{N_{s\phi}(\theta_r)}{D_\phi(\theta_r)} \text{ and } c\phi_r = \frac{N_{c\phi}(\theta_r)}{D_\phi(\theta_r)} \quad (27)$$

with

$$\begin{aligned}N_{s\phi}(\theta_r) = {}&e_{33}^d\left[(e_{31}^c)^2 c^2\theta_r - (e_{32}^c)^2 s^2\theta_r\right] + e_{33}^c\\ &\left[-e_{31}^c e_{31}^d + e_{32}^c e_{32}^d - (e_{32}^c)^2 c^2\theta_r + (e_{31}^c)^2 s^2\theta_r\right]\end{aligned} \quad (28)$$

,

$$\begin{aligned}N_{c\phi}(\theta_r) = {}&e_{33}^c e_{33}^d(e_{31}^c c\theta_r - e_{32}^c s\theta_r) + (e_{31}^c c\theta_r +\\ &e_{32}^c s\theta_r)\left[e_{31}^c e_{31}^d - e_{32}^c e_{32}^d + (e_{32}^c)^2 c^2\theta_r - (e_{31}^c)^2 s^2\theta_r\right]\end{aligned} \quad (29)$$

and

$$D_\phi(\theta_r) = (e^c_{31}c\theta_r - e^c_{32}s\theta_r)\left[(e^c_{31}c\theta_r + e^c_{32}s\theta_r)^2 + (e^c_{33})^2\right] \quad (30)$$

From the system of equations (27), the expression of ϕ_r is deduced as follows:

$$\phi_r = a\tan 2\left[N_{s\phi}(\theta_r), N_{c\phi}(\theta_r)\right] \quad (31)$$

3) **Calculation of α_r:** Equations (16) and (17) can be transformed into a system of equations as follows:

$$\begin{cases} N_{1\alpha}(\theta_r,\phi_r)c\alpha_r - N_{2\alpha}(\theta_r,\phi_r)s\alpha_r = e^d_{13} \\ N_{2\alpha}(\theta_r,\phi_r)c\alpha_r + N_{1\alpha}(\theta_r,\phi_r)s\alpha_r = e^d_{23} \end{cases} \quad (32)$$

with

$$\begin{cases} N_{1\alpha}(\theta_r,\phi_r) = e^c_{11}c\theta_r s\phi_r + e^c_{12}s\theta_r s\phi_r + e^c_{13}c\phi_r \\ N_{2\alpha}(\theta_r,\phi_r) = e^c_{21}c\theta_r s\phi_r + e^c_{22}s\theta_r s\phi_r + e^c_{23}c\phi_r \end{cases} \quad (33)$$

Solving this system (32) leads to the following expressions for $s\alpha_r$ and $c\alpha_r$:

$$\begin{cases} s\alpha_r = \frac{-e^d_{13}N_{2\alpha}(\theta_r,\phi_r)+e^d_{23}N_{1\alpha}(\theta_r,\phi_r)}{[N_{1\alpha}(\theta_r,\phi_r)]^2+[N_{2\alpha}(\theta_r,\phi_r)]^2} \\ c\alpha_r = \frac{e^d_{13}N_{1\alpha}(\theta_r,\phi_r)+e^d_{23}N_{2\alpha}(\theta_r,\phi_r)}{[N_{1\alpha}(\theta_r,\phi_r)]^2+[N_{2\alpha}(\theta_r,\phi_r)]^2} \end{cases} \quad (34)$$

From the system of equations (34), the expression of α_r is deduced as follows:

$$\alpha_r = a\tan 2\left[\begin{array}{l} -e^d_{13}N_{2\alpha}(\theta_r,\phi_r) + e^d_{23}N_{1\alpha}(\theta_r,\phi_r), \\ e^d_{13}N_{1\alpha}(\theta_r,\phi_r) + e^d_{23}N_{2\alpha}(\theta_r,\phi_r) \end{array}\right] \quad (35)$$

4) **Calculation of λ_r, X_{Gr} and Y_{Gr}**: The equations (21),(19) and (20) allow to calculate λ_r, X_{Gr} and Y_{Gr} respectively as follows:

$$\begin{cases} \lambda_r = \frac{Z_d - Z_c - Z_G}{E_3(\theta_r,\phi_r)} \\ X_{Gr} = X_d - E_1(\theta_r,\phi_r,\alpha_r,\lambda_r) \\ Y_{Gr} = Y_d - E_2(\theta_r,\phi_r,\alpha_r,\lambda_r) \end{cases} \quad (36)$$

B. effectiveness analysis of the proposed mathematical solution

In this paper, the development of the FKM (9) leads to 12 equations. However, 8 (12, 15-21) of these 12 equations were used to solve the IK. Thus, when the inertial paremeters are neglected and the continuum manipulator is cylindrical in shape, the EE pose error will always be zero if the expressions of θ_r (24), ϕ_r (31) and α_r (35) are also solutions of equations (10, 11, 13 and 14) not used to establish the proposed mathematical solution. In this paper, the verification of these equations consists first in expressing in terms of euler's parameters e^k_l ($l = 0, ..., 3, k = c, d$) of $c\theta_r$, and higher degrees of $c\theta_r$, the expressions for :

1) e^k_{ij} ($i = 1, 2, 3$, $j = 1, 2, 3$ and $k = c, d$) as follows:

$$\begin{cases} e^k_{ii} = (e^k_0)^2 + (e^k_i)^2 - 1/2 \\ e^k_{12} = e^k_1e^k_2 - e^k_0e^k_3 \\ e^k_{13} = e^k_1e^k_3 + e^k_0e^k_2 \\ e^k_{21} = e^k_1e^k_2 + e^k_0e^k_3 \\ e^k_{23} = e^k_2e^k_3 - e^k_0e^k_3 \\ e^k_{31} = e^k_1e^k_3 - e^k_0e^k_2 \\ e^k_{32} = e^k_2e^k_3 + e^k_0e^k_3 \end{cases} \quad (37)$$

with $(e^k_0)^2 + (e^k_1) + (e^k_2)^2 + (e^k_3)^2 = 1$

2) $s\theta_r$ from equations (24 and 37)
3) $s\phi_r$ and $c\phi_r$ from equations (27-30,24 and 37).
4) $s\alpha_r$ and $c\alpha_r$ from equations (34,33,27-30,24 and 37)

Then, these expressions are replaced in the equations (10,11,13 and 14) and show that θ_r, ϕ_r and α_r are solution of these equations. The computations were performed using symbolic calculation in matlab software and took about 40 hours on a Intel® Core™ i7-1195G7 at 16 GB DDR4-3200 SDRAM (2 x 8 GB) and 512 GB PCIe® NVMe™ M.2 SSD.

IV. SIMULATIONS AND RESULTS

This section focuses on the validation of the proposed mathematical solution via simulations. The purpose of this simulation is to show the applicability of the proposed mathematical solution on a virtual SSMCM. The performance of the proposed mathematical solution is evaluated on a difficult path described by a spiral wave of equation:

$$\begin{cases} x \in [-2000; 2000] \\ y = 350 + 50\sin(-\omega x), \quad \omega = \pi/500 \\ z = 450 + 50\cos(-\omega x) \end{cases} \quad (38)$$

The mobile platform has a radius of 185 mm. The continuum manipulator has a single section with a radius of 50 mm, a minimum actuator length of 250 mm and a maximum actuator length of 450 mm. Tracking of this path (38) was performed with an EE orientation of $[e_0, e_1, e_2, e_3] = [0.97, 0.092, 0.126, -0.054]$ and the results obtained are presented in Fig. 2 and available on the video [12]. The variations of the actuator lengths presented in Fig. 3 are continuous and thus show the efficiency of the proposed mathematical model. Furthermore, Table I shows the maximum Euclidean errors and the computation time between the proposed mathematical solution based IKM (MSIKM), the CIKM [9] and the Lagrange multiplier based IKM (LMIKM) [9]. We note that the maximum Euclidean error of the proposed MSIKM is zero compared to the CIKM and LMIKM which are close to ± 1.5mm for position and ± 0.0138 for orientation. Note that the computation time is low for the proposed MSIKM and CIKM, 15 and 19 seconds respectively, compared to the LMIKM which has a high computation time of 108 seconds. On the other hand, the CIKM results were obtained with a database of 232,925 samples, with discretisation steps of 20mm, 100mm and 60°for the actuator length, platform position parameters and platform orientation, respectively.

TABLE I
SIMULATIONS: MAXIMUM EUCLIDEAN ERROR (POSITIONS IN MM) AND COMPUTING TIME (SECONDS).

Methods	X	Y	Z	e_0	e_1	e_2	e_3	T
MSIKM	0	0	0	0	0	0	0	15
CIKM [9]	1.3973	1.0783	0.9037	0.0022	0.0137	0.0082	0.0073	26
LMIKM [9]	0.9513	1.4709	1.1351	0.0014	0.0138	0.0125	0.0109	108

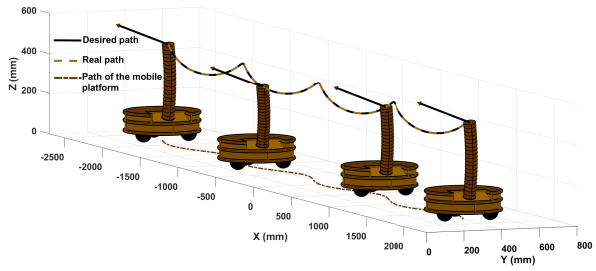

Fig. 2. Simulation: Tracking of a spiral wave path by a SSMCM.

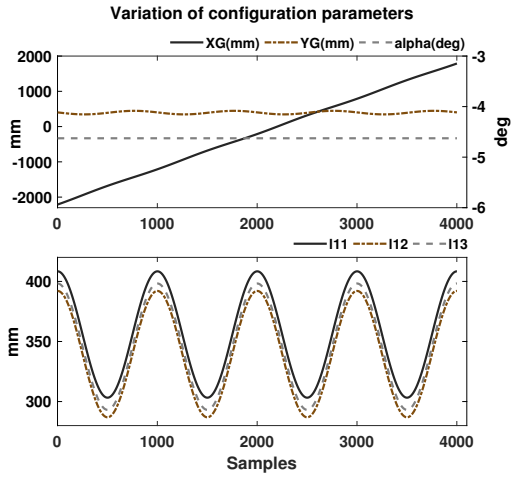

Fig. 3. Simulation: Variation of the configurations parameters.

V. EXPERIMENTS AND RESULTS

This section presents the implementation of the proposed mathematical solution on a MCM called Robotino XT. Since the robot has two sections, we combined the proposed mathematical solution with the CIKM developed in [9].Thus, the section starts with the description of the experimental platform, followed by the clustering phase. It ends with the presentation of the experiments and the results obtained and a discussion.

A. Description of Robotino XT

The Robotino XT shown in Fig. 4. is a mobile platform called Robotino and a manipulator with two continuum sections called the Compact Bionic Handling Assistant (CBHA). Each section of the CBHA is controlled by three pneumatic tubes supplied with pressure under the control of a proportional-integrator-derivative (PID) controller. A wrist pin with a flexible clamp is attached to the end of the second section. Below the first section is a mobile platform consisting of three independent omnidirectional drive units placed at an angle of 120° from each other.

B. Generation of the learning database and Clustering

The proposed mathematical solution can be applied to the MCM with with N sections, only when the values of the actuator lengths of the $(N-1)$ sections are known. In this paper, the CIKM developped in [9] is used to parameterize the $(N-1)$ sections in order to avoid the limit actuator lengths after calculating the configuration space parameters of the unparameterized section by the proposed mathematical solution.

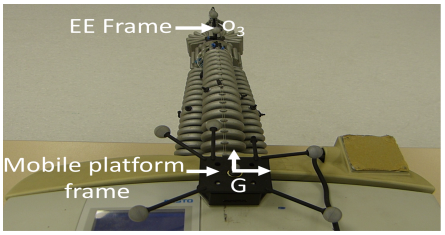

Fig. 4. Data collection experimental setup.

The clustering involves a learning database. This last can be contructed from the CCA-based FKM. However, the conical shape and dynamic uncertainties of the robot lead to inaccurate CCA-based FKMs [13]. Thus, the learning database of the CBHA is first built experimentally using the motion tracking system, and the database of the Robotino XT is deduced after that using the HTMs. The data collection setup is given in Fig.4. The exploration of the CBHA's workspace is done by supplying the pressure into six CBHA's pneumatic actuators. The input signals are obtained by discretizing the pressure variable with a step size of 0.5 bar. With a range of pressure varying of 0 to 2 bars, the six tubes allow to obtain a learning database of CBHA of 15625 samples in approximately 6 hours. With a range of α from -180° to 180° and a step size of 90°, the learning database of the RobotinoXT has 78125 samples. Note that the values of X_G and Y_G are zero.

The clustering is performed using the GNG algorithm. The following GNG's parameters $\lambda = 100$, $\alpha_t = 0.5$, $\varepsilon_n = 0.009$ and $\varepsilon_b = 0.3$ have achieved satisfactory performance. They are obtained in using the genetic algorithm [14]. The details on the GNG algorithm are referred to [9] and [15].

C. Experimental results and discussions

The proposed approach is validated by implementing it on the Robotino XT, as shown in Fig. 5. The actuator lengths and mobile platform values provided by the proposed mathematical solution are tracked by two independent controllers developed in [16] and [17], respectively. The EE pose of the Robotino XT $[X_*, Y_*, Z_*, e_0^*, e_1^*, e_2^*, e_3^*]^T$ is tracked by the Optitrack motion system and compared to the desired pose $[X_d, Y_d, Z_d, e_0^d, e_1^d, e_2^d, e_3^d]^T$ in real-time. The Optitrack motion system comprises eight cameras and can track rigid body movement reliably up to $\pm 0.1mm$.

The experiment evaluates the performance of the proposed mathematical solution on a linear path. This environment contains a gray metal bar (obstacle) that the robot must avoid. The desired path of equation

$$\begin{cases} x \in [0; 2000]\,\text{mm} \\ y = 350\text{mm} \\ z = 130\text{mm} \end{cases} \tag{39}$$

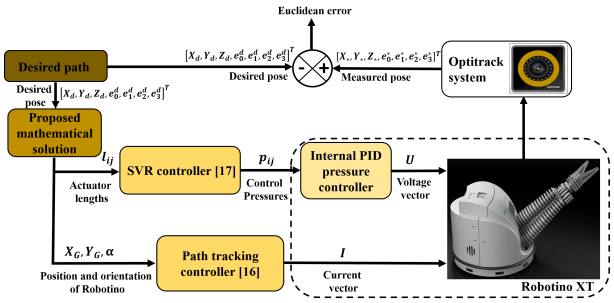

Fig. 5. Experimental setup for validation of the proposed mathematical solution

The tracking is performed with an EE orientation $[e_0, e_1, e_2, e_3] = [0.923, -0.382, 0, 0]$ as shown Fig.6 and the video available in [18]. However, the orientation is modified at $[e_0, e_1, e_2, e_3] = [0.976, -0.216, 0, 0]$ for allowing to the robot to avoid the obstacle. The associated Euclidean position errors are provided in Fig.7. The proposed method is compared with the CIKM and the results are presented in the Table II. We observe that the maximum Euclidean errors of the proposed MSIKM are ± 6.5mm in position and ± 0.0518 in orientation and are lower than those of the CIKM which are ± 10mm in position and ± 0.0769 in orientation. However, the computation time is almost similar, with 220 and 229 seconds for the MSIKM and CIKM respectively. On the other hand, Fig.8 present the variation of the configurations parameters of the Robotino XT. Some discontinuities observed are due to the presence of obstacles.

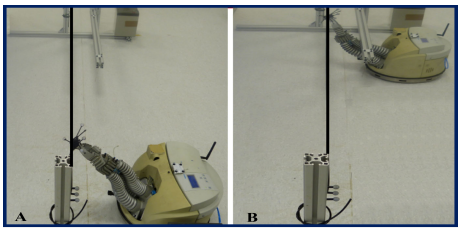

Fig. 6. Experiment:tracking the Robotino XT tracks a linear wave path in avoiding the gray metal bar.

TABLE II
EXPERIMENTS: EUCLIDEAN ERROR (POSITIONS IN MM) AND COMPUTING TIME (SECONDS).

Methods	X	Y	Z	e_0	e_1	e_2	e_3	T
MSIKM	4.8280	6.2560	4.6867	0.0105	0.0507	0.0506	0.0518	220
CIKM [9]	7.9640	9.7280	6.0489	0.0132	0.0769	0.0655	0.0614	229

In summary, from the results obtained, we can conclude that the proposed mathematical solution effectively solves the IK of an SSMCM. It can be combined with CIKM to solve the IK of an extensible multisection MCM. This combination leads to several IK solutions and allows the MCM to operate in restricted environments, as illustrated in the video [19]. While the simulations show that there are no EE pose errors,

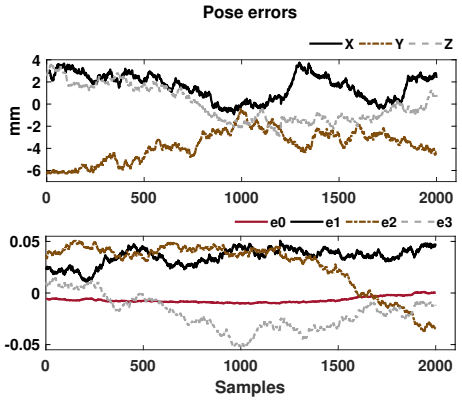

Fig. 7. Experiment: pose errors.

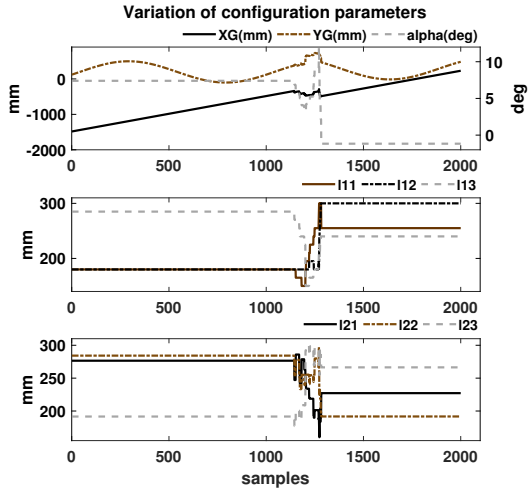

Fig. 8. Experiment: variation of the configurations parameters.

the presence of EE pose errors in the experimentation is due to the inaccuracy of the independent controllers developed in [16], [17] and the uncertain robot dynamics. Comparisons with existing approaches show that the proposed MSIKM has a high accuracy and a very fast computation time. On the other hand, the proposed mathematical solution can also be applied on the non-extensible SSMCM using the mobile platforms such as the hexapod robot, the universal aerial vehicle or a mobile platform on which is placed a frame that moves vertically as shown in the video available in [20].

VI. CONCLUSION

This paper solves the IK of the SSMCM using a new mathematical solution. The approach consists of determining the configuration parameters of a single section of the continuum manipulator and the pose parameters of the mobile platform. Experiments performed on the Robotino XT show that it will be interesting to develop in future works robust control laws that integrate the robot dynamics model, to further minimize the Cartesian errors.

REFERENCES

[1] A. J. Kouabon, A. Melingui, J. M. Ahanda, O. Lakhal, V. Coelen, M. KOM, and R. Merzouki, "A learning framework to inverse kinematics of high dof redundant manipulators," *Mechanism and Machine Theory*, vol. 153, p. 103978, 2020.

[2] I. M. Loutfi, A. B. Boutchouang, A. Melingui, O. Lakhal, F. B. Motto, and R. Merzouki, "Learning-based approaches for forward kinematic modeling of continuum manipulators," *IFAC-PapersOnLine*, vol. 53, no. 2, pp. 9899–9904, 2020.

[3] R. Bogue, "Robots in the nuclear industry: a review of technologies and applications," *Industrial Robot: An International Journal*, 2011.

[4] G. Methenitis, D. Hennes, D. Izzo, and A. Visser, "Novelty search for soft robotic space exploration," in *Proceedings of the 2015 annual conference on Genetic and Evolutionary Computation*. ACM, 2015, pp. 193–200.

[5] Y. Sun, A. Abudula, H. Yang, S.-S. Chiang, Z. Wan, S. Ozel, R. Hall, E. Skorina, M. Luo, and C. D. Onal, "Soft mobile robots: A review of soft robotic locomotion modes," *Current Robotics Reports*, vol. 2, pp. 371–397, 2021.

[6] W. McMahan, V. Chitrakaran, M. Csencsits, D. Dawson, I. D. Walker, B. A. Jones, M. Pritts, D. Dienno, M. Grissom, and C. D. Rahn, "Field trials and testing of the octarm continuum manipulator," in *Proceedings 2006 IEEE International Conference on Robotics and Automation, 2006. ICRA 2006.* IEEE, 2006, pp. 2336–2341.

[7] J. Liu, S. Iacoponi, C. Laschi, L. Wen, and M. Calisti, "Underwater mobile manipulation: A soft arm on a benthic legged robot," *IEEE Robotics & Automation Magazine*, vol. 27, no. 4, pp. 12–26, 2020.

[8] J. Li and J. Xiao, "A general formulation and approach to constrained, continuum manipulation," *Advanced Robotics*, vol. 29, no. 13, pp. 889–899, 2015.

[9] A. H. B. Boutchouang, A. Melingui, J. J.-B. M. Ahanda, O. Lakhal, F. B. Motto, and R. Merzouki, "Learning-based approach to inverse kinematics of wheeled mobile continuum manipulators," *IEEE-ASME TRANSACTIONS ON MECHATRONICS*, 2022.

[10] L. Guilamo, J. Kuffner, K. Nishiwaki, and S. Kagami, "Efficient prioritized inverse kinematic solutions for redundant manipulators," in *2005 IEEE/RSJ International Conference on Intelligent Robots and Systems*. IEEE, 2005, pp. 3921–3926.

[11] C. Escande, R. Merzouki, P. M. Pathak, and V. Coelen, "Geometric modelling of multisection bionic manipulator: Experimental validation on robotinoxt," in *Robotics and Biomimetics (ROBIO), 2012 IEEE International Conference on*. IEEE, 2012, pp. 2006–2011.

[12] A. H. B. Boutchouang, "Simulation: Tracking of a spiral wave path by a single section mobile continuum manioulator." 2022, visited on 15 September 2022. [Online]. Available: https://youtu.be/_ztIxwlumOQ

[13] A. B. Boutchouang, A. Melingui, J. M. Ahanda, O. Lakhal, F. B. Motto, and R. Merzouki, "Forward kinematic modeling of conical-shaped continuum manipulators," *Robotica*, vol. 39, no. 10, pp. 1760–1778, 2021.

[14] J. H. Holland, "Genetic algorithms," *Scientific american*, vol. 267, no. 1, pp. 66–73, 1992.

[15] B. Fritzke, "A growing neural gas network learns topologies," in *Advances in neural information processing systems*, 1995, pp. 625–632.

[16] G. Klancar, D. Matko, and S. Blazic, "Mobile robot control on a reference path," in *Proceedings of the 2005 IEEE International Symposium on, Mediterrean Conference on Control and Automation Intelligent Control, 2005.* IEEE, 2005, pp. 1343–1348.

[17] A. Melingui, J. J.-B. M. Ahanda, O. Lakhal, J. B. Mbede, and R. Merzouki, "Adaptive algorithms for performance improvement of a class of continuum manipulators," *IEEE Transactions on Systems, Man, and Cybernetics: Systems*, vol. 48, no. 9, pp. 1531–1541, 2017.

[18] A. H. B. Boutchouang, "Experiment: Tracking of a linear wave path by a two-section mobile continuum manioulator," 2022, visited on 15 September 2022. [Online]. Available: https://youtu.be/GtEDrlf-180

[19] ——, "Simulation: A three-section mobile continuum manioulator moves a white bottle from the gray table to the gray cupboard." 2022, visited on 15 September 2022. [Online]. Available: https://youtu.be/QCKNR5knnWA

[20] ——, "Simulation: Tracking of a spiral wave path by a non-extensible single section mobile continuum manipulator." 2022, visited on 21 october 2022. [Online]. Available: https://youtu.be/3WD1KOqsHaM